#140

Phys Chem Minerals (1990) 17:228–237

PHYSICS AND CHEMISTRY OF MINERALS

High-Pressure Crystal Chemistry of $MgSiO_3$ Perovskite

Nancy L. Ross* and Robert M. Hazen

Geophysical Laboratory, Carnegie Institution of Washington, 5251 Broad Branch Road, NW, Washington, DC 20015, USA

Received September 2, 1989

Abstract. A high-pressure single-crystal x-ray diffraction study of perovskite-type $MgSiO_3$ has been completed to 12.6 GPa. The compressibility of $MgSiO_3$ perovskite is anisotropic with b approximately 23% less compressible than a or c which have similar compressibilities. The observed unit cell compression gives a bulk modulus of 254 GPa using a Birch-Murnaghan equation of state with K' set equal to 4 and V/V_0 at room pressure equal to one. Between room pressure and 5 GPa, the primary response of the structure to pressure is compression of the Mg–O and Si–O bonds. Above 5 GPa, the SiO_6 octahedra tilt, particularly in the [bc]-plane. The distortion of the MgO_{12} site increases under compression. The variation of the O(2)–O(2)–O(2) angles and bond-length distortion of the MgO_{12} site with pressure in $MgSiO_3$ perovskite follow trends observed in $GdFeO_3$-type perovskites with increasing distortion. Such trends might be useful for predicting distortions in $GdFeO_3$-type perovskites as a function of pressure.

Introduction

Synthesis and characterization of silicate perovskites have presented a formidable challenge to mineral physics researchers since Ringwood (1962, 1966) first noted the possible importance of $MgSiO_3$ and $CaSiO_3$ perovskites in lower mantle petrology. Several workers subsequently demonstrated high-pressure transformations from pyroxene and garnet structures to perovskite in analog systems, including Ca(Ge, Si)O_3 and Ca(Ti, Si)O_3 (Marezio et al. 1966; Ringwood and Major 1967, 1971; Reid and Ringwood 1975). Pure silicate perovskites of composition $MgSiO_3$ and $CaSiO_3$ were prepared by Liu and Ringwood (1975) and Liu (1974; 1975a, b; 1976a–c), and laboratories in Japan and the United States soon duplicated the Australian results (Sawamoto 1977; Ito 1977; Ito and Matsui 1977, 1978, 1979; Mao et al. 1977). By the late 1970s many geophysicsts were convinced that the 650 km mantle seismic discontinuity coincides with a perovskite phase transition boundary, and that (Mg, Fe)SiO_3 perovskite is a dominant lower mantle mineral (Anderson 1976; Liu 1977, 1979; Yagi et al. 1979). Characterization of silicate perovskite became a major objective of scientists interested in the deep earth.

The first experimental studies of silicate perovskite properties relied on microgram quantities of polycrystalline $MgSiO_3$. Yagi et al. (1978, 1982) documented the perovskite's room-pressure orthorhombic crystal structure and room-temperature compressibility. Other workers reported thermal conductivity (Knittle et al. 1986), electrical conductivity (Li and Jeanloz 1987), and vibrational spectroscopy (Weng et al. 1983; Williams et al. 1987; Hofmeister et al. 1987). Recent phase equilibria investigators have focused on the ternary MgO–FeO–SiO_2 system, especially for assumed mantle compositions near $Mg_{0.9}Fe_{0.1}SiO_3$ (Yagi et al. 1979; Ito 1982; Ito et al. 1984; Heinz and Jeanloz 1987; Jackson et al. 1987; Knittle and Jeanloz 1987).

Present experimental limitations generally preclude measurement of silicate perovskite properties at the extreme mantle temperatures and pressures of synthesis. Computer modeling of $MgSiO_3$ and $CaSiO_3$ has proven an attractive alternative for obtaining estimates of perovskite structures and properties. Computational techniques based on nearest-neighbor interactions were employed by Ito and Matsui (1978) and Miyamoto and Takeda (1984) to predict structural parameters. More recent calculations have focused on the elasticity and equations of state of endmember magnesium and calcium silicate perovskites. Lattice-dynamical calculations using empirical potentials provided estimates of elastic properties (Matsui et al. 1987; Choudhury et al. 1988) as well as defect energies (Wall et al. 1986) and ion migration paths (Miyamoto 1988). Models based on ab initio potentials (non-empirical, in the sense that interatomic potentials do not depend on experimental data) have also been applied to silicate perovskites by Wolf and

* Present address: Department of Geological Sciences, University College London, Gower Street, London WC1E 6BT, UK

Bukowinski (1985, 1987), Hemley et al. (1987), Cohen (1987), and Hemley et al. (1989). The latter study is particularly successful in reproducing experimental values of room-pressure structure parameters and elastic moduli.

Ito and Weidner's (1986) synthesis of single crystal $MgSiO_3$ perovskite up to 300 μm diameter represented an important advance. Single crystals, unlike powdered samples, facilitate the measurement of anisotropic structural and physical properties. The Ito and Weidner samples have allowed the precise measurement of crystal structure at room conditions (Horiuchi et al. 1987) and high pressure (Kudoh et al. 1987), elastic moduli (Yeganeh-Haeri et al. 1989), thermal expansion (Ross and Hazen 1989), and vibrational spectra (Hemley et al. 1989).

In spite of these improved samples, however, there remains considerable uncertainty regarding the behavior of $MgSiO_3$ perovskite at high pressure. Yagi et al. (1982), for example, determined the following order for the compressibilities of the lattice parameters: $a > b \approx c$ and calculated an isothermal bulk modulus of 258 GPa. Knittle and Jeanloz (1987) found $c \approx b \approx a$ and $K_T = 266$ GPa. Results from Kudoh et al.'s (1987) single-crystal study are $c > a > b$ and $K_T = 247$ GPa. Single-crystal Brillouin spectroscopy by Yeganeh-Haeri et al. (1990) suggest $c > a > b$ and an adiabatic bulk modulus of 246 GPa. Recently, Mao et al. (1989) found $c > a > b$ and $K_T = 272$ GPa.

We undertook a single-crystal x-ray diffraction study of $MgSiO_3$ perovskite to 12.6 GPa in order to resolve these differences. Since the compression results are sensitive to non-hydrostatic stresses, two hydrostatic pressure media were employed this study: the first, a 4:1 methanol:ethanol solution was used for studies to 5 GPa, while the second medium, neon, was used in runs exceeding 6 GPa. Trends in the axial compressibilities and isothermal bulk modulus are reported and compared with results from the previous studies. In addition, the subtle changes in the structure of $MgSiO_3$ perovskite with increasing pressure are described and compared with other $GdFeO_3$-type perovskites.

Experimental

The single crystals of $MgSiO_3$ perovskite, synthesized at 22 GPa and 1000° C in the presence of a small amount of water (Ito and Weidner 1986), were generously provided by Dr. E. Ito of Okayama University, Japan. We examined a dozen crystals with a precession camera and an automated four-circle diffractometer and selected three untwinned samples for high-pressure study. The peak profiles were broad in all three of the crystals, possibly due to a small mosaic size formed upon quenching from high pressure and temperature. Crystal # 1, a 80 × 80 × 40 μm plate, was mounted in a triangular Merrill-Bassett type diamond-anvil cell with an Inconel 750X gasket (350 μm-diameter hole). The perovskite crystal and several 10 μm chips of ruby pressure calibrant were afixed to one diamond face with a thin smear of the alcohol-insoluble fraction of vaseline, and a 4:1 mixture of non-dried methanol:ethanol was the hydrostatic pressure-transmitting medium. Procedural details of crystal mounting, pressure calibration, and cell operation are given by Hazen and Finger (1982). Perovskite crystal # 1 was oriented with the (210) direction perpendicular to the anvil faces; thus the c axis was parallel to the diamonds.

Table 1. Cell parameters and volume of $MgSiO_3$ perovskite

P (GPa)	a (Å)	b (Å)	c (Å)	Vol. (Å^3)	Ref.
0.001	4.7754 (3)	4.9292 (4)	6.8969 (5)	162.35 (2)	1
0.001	4.7787 (4)	4.9313 (4)	6.9083 (8)	162.80 (3)	2
0.001	4.774 (1)	4.929 (5)	6.903 (4)	162.4 (2)	3
0.001	4.777 (2)	4.927 (1)	6.89772 (9)	162.36 (7)	4
1.0	4.768 (3)	4.922 (2)	6.8898 (15)	161.69 (12)	4
2.2	4.762 (1)	4.918 (1)	6.8767 (9)	161.03 (6)	4
3.0	4.758 (2)	4.911 (3)	6.8680 (14)	160.46 (9)	4
3.5	4.754 (2)	4.911 (2)	6.8653 (12)	160.30 (8)	4
5.0	4.746 (2)	4.899 (3)	6.8538 (16)	159.34 (10)	4
0.01	4.774 (2)	4.9262 (6)	6.8927 (6)	162.10 (5)	5
1.7	4.761 (2)	4.9148 (7)	6.8760 (7)	160.89 (6)	5
2.5	4.759 (1)	4.9134 (6)	6.8714 (6)	160.67 (5)	5
3.3	4.752 (1)	4.9096 (6)	6.8637 (6)	160.14 (5)	5
3.8	4.750 (1)	4.9071 (6)	6.8596 (6)	159.88 (5)	5
3.9	4.7495 (6)	4.9066 (3)	6.8590 (3)	159.84 (2)	5
0.01	4.778 (2)	4.933 (1)	6.9010 (6)	162.65 (7)	6
5.5	4.745 (3)	4.903 (3)	6.8550 (13)	159.47 (11)	6
10.8	4.710 (1)	4.873 (1)	6.8079 (26)	156.26 (8)	6
6.5	4.735 (1)	4.895 (1)	6.843 (3)	158.61 (8)	7
7.5	4.7321 (8)	4.892 (1)	6.836 (2)	158.22 (6)	7
10.6	4.710 (1)	4.873 (2)	6.807 (3)	156.24 (9)	7
12.6	4.698 (2)	4.866 (2)	6.790 (4)	155.23 (12)	7

References: 1. Ito and Matsui (1978); 2. Horiuchi et al. (1987); 3. Kudoh et al. (1987) (in diamond anvil cell); 4. This study, crystal # 1; 5. This study, crystal # 1 + fluorite; 6. This study, crystal # 2; 7. This study, crystal # 3

Unit-cell parameters were obtained at 0.94, 2.2, 3.0, 3.5, and 5.0 GPa as well as at room-pressure while the crystal was still mounted in the cell. At each pressure from 16 to 20 reflections with $20° < 2\Theta < 30°$ were centered at eight equivalent positions following the procedure of King and Finger (1979). Initial unit-cell refinements were made without constraints (i.e., as triclinic) to test for deviations from orthorhombic dimensionality. All unit-cell angles at all pressures were 90° within two estimated standard deviations. Final cell parameters, recorded in Table 1, were calculated with orthorhombic constraints (Ralph and Finger 1982). Full sets of intensity data were collected at 0.0, 2.2 and 5.0 GPa with the crystal still in the diamond cell.

Crystal # 1 was dismounted and remounted in the Merrill-Bassett cell in the same approximate orientation, but with the addition of 150 × 150 × 10 μm-thick single crystal of fluorite (CaF_2), which was fixed against one diamond anvil face and served as a second internal pressure standard (Hazen and Finger 1981). Unit-cell data were obtained at 1.72, 2.51, 3.33, 3.76, and 3.86 GPa as well as at room pressure in the diamond cell.

Crystal # 2, a 30 × 30 × 20 equant fragment, was selected for study in a diamond cell designed to use solidified gas as the pressure medium (Mills et al. 1980; Jephcoat et al. 1987). This four-screw cell, which features opposite pairs of screws oppositely threaded for uniform pressurization, is suitable for x-ray diffraction studies of single crystal to above 20 GPa (Hazen and Finger 1982). Perovskite crystal # 2 and ruby fragments were mounted against one diamond face and enclosed by a preindented Inconel gasket with 200 μm-diameter hole. The crystal was oriented with 110 perpendicular to the anvil faces. We placed the cell, slightly opened, in a steel bomb, which was pressurized to 0.2 GPa with neon gas. The diamond cell seals by a remote-controlled motorized gear assembly, and cell operation then procedes in the normal manner.

Unit-cell parameters were obtained at 5.5 and 10.8 GPa, as well as at room pressure, but the crystal proved too small (i.e.,

peak-to-background ratios were too low) for meaningful collection of intensity data. This difficulty is inherent in single-crystal studies at pressures above 10 GPa; crystals must be less than 25 μm thick to prevent crushing, and the beryllium backing pieces must be thicker to support the diamonds. Thus, peak-to-background ratios are often small in high-pressure single crystal experiments.

Crystal # 3, a $35 \times 40 \times 25$ μm plate flattened in the (001) plane was mounted in the gas cell with neon as the pressure medium. Angular measurements for unit-cell determinations were obtained at 6.5, 7.5, 10.6 and 12.6 GPa and complete sets of intensity data were obtained at 7.5 and 10.6 GPa. Unfortunately, crystal # 3 was crushed between the diamond anvils in an effort to attain 15 GPa, so no room-pressure information in the cell could be obtained for that crystal. It appears, given the inevitable tradeoff between crystal size and maximum attainable pressure, that 15 GPa represents an approximate pressure limit for the study of single-crystal $MgSiO_3$ perovskite with a conventional sealed X-ray source.

Monochromatized Mo Kα radiation ($\lambda = 0.7107$ Å) was used for all the diffraction-intensity measurements. All accessible reflections, including crystallographically equivalent reflections, to $\sin\Theta/\lambda \leq 0.7$, were obtained by the ω-scan technique using a Huber four-circle diffractometer. Intensity data were collected in the Merrill-Bassett diamond anvil cell with 0.025° steps and 4.0 second-per-step counting times; 0.020° steps and 20.0 second-per-step counting times were used for collection of intensity data in the gas-cell. Corrections were made for Lp effects and absorption by the components of the diamond anvil cell. No correction was made for absorption by the crystal because of the sufficiently small value of μ (14.07 cm^{-1}). In all of the data collections, the systematic absences were consistent with space group P *bnm*. Refinements were carried out with RFINE4 (Finger and Prince 1974) applying the weight of $1/(\sigma^2_{hkl} + (0.01\ F_{obs})^2)$ for each reflection. The refinements were initiated with the atomic coordinates of Horiuchi et al. (1987) and complex scattering factors for neutral atoms were taken from the International Tables for X-ray Crystallography (1974). Conditions of refinement and refined structural parameters are recorded in Table 2 and 3, respectively. Bond lengths and angles are presented in Tables 5, 6 and 7.

Table 2. Summary of data collections and refinements

Pressure (GPa):	0.001	2.2	5.0	7.5	10.6
Crystal #	1	1	1	3	3
No. of symmetry-equivalent reflections with $I > 3\sigma_I$	113	96	95	75	80
R_{int} of symmetry-equivalent reflections for averaging	0.033	0.047	0.045	0.052	0.069
R	0.042	0.036	0.052	0.040	0.062
R_w	0.029	0.030	0.049	0.025	0.042
G.O.F.	1.04	1.22	1.96	0.99	1.97

Results and Discussion

Systematic Errors in High-Pressure Studies

Single-crystal diamond cell experiments are subject to a number of systematic errors. Only about a third of reciprocal space is accessible, so any data set is initially biased, with crystallographic axes and structural parameters perpendicular to the diamond anvil faces less well constrained than those parallel to the faces. Other problems intrinsic to a diamond-cell experiment include non-uniform absorption by beryllium and diamond components of the cell, shielding of off-center crystals by the x-ray-opaque gasket, and possible crystal deformation at high pressure due to non-hydrostatic media. These difficulties can be recognized, and for the most part eliminated, by always measuring the crystal's unit cell and structure at room pressure in the diamond cell. These reference unit-cell and structure data must be obtained using the same experimental conditions (e.g., the same set of reflections for unit-cell refinement) as at high pressure. Only in this way can meaningful comparisons between room and high pressure behavior be ascertained.

Previous high-pressure studies reveal the dangers of combining conventional room-pressure data with diamond cell high-pressure data. Hazen and Finger (1978), for example, obtained pyrope and grossular garnet compressibilities that were almost 20% too high (Levien et al. 1979) because they used precise room-pressure lattice parameters measured with high-angle reflections on crystals in air. Those room-pressure data were combined with high-pressure unit-cell parameters obtained by centering low-angle peaks. Systematic diffractometer errors resulted in the room-pressure values appearing too large relative to high-pressure values (Swanson et al. 1985); thus, the calculated bulk moduli were too low.

In this study, unit cell parameters and intensity data were obtained, whenever possible, at room pressure and temperature in the diamond anvil cell. The refined positional parameters from data collected at room-pressure in the diamond anvil cell show good agreement with Horiuchi et al.'s (1987) results (Table 3). The largest discrepancy between the two studies is in the *z*-coordinate of O(2), illustrating that structural parameters perpendicular to the diamond anvil faces are less well constrained than those parallel to the faces. The unit cell parameters also show excellent agreement with those of previous studies (Table 1) and show similar variations, especially in *b* and *c*. Special care was taken to use the same set of reflections to determine the cell parameters at pressure. For different mounts with crystals in different orientations, reflections in the same 2θ range were chosen for the lattice determinations. Unfortunately, we were unable to collect a cell at room pressure and temperature for crystal # 3. Values of the lattice parameters at room pressure, obtained from linear regressions of the high-pressure data ($a = 4.778$ Å, $b = 4.928$ Å and $c = 6.899$ Å), are in excellent agreement with crystal # 1 (Table 1). Moreover, systematic errors are minimized for higher-pressure data because the magnitude of changes are much larger and are less influenced by small errors in room-pressure values.

$MgSiO_3$-Perovskite Axial Compressibilities

The three crystals in this study, loaded with different orientations in the diamond anvil cell and with different pressure media, displayed anisotropic behavior as a function pressure of pressure. We found that the *b*-axis was

Table 3. Refined atomic coordinates and isotropic temperature factors

Pressure (GPa):		0.001[a]	0.001[b]	2.2	5.0	7.7	10.6
Mg	x	0.5141 (1)	0.5131 (7)	0.5155 (8)	0.5151 (14)	0.5138 (9)	0.5114 (16)
	y	0.5560 (1)	0.5563 (4)	0.5573 (5)	0.5558 (8)	0.5567 (5)	0.5566 (9)
	z	0.2500	0.2500	0.2500	0.2500	0.2500	0.2500
	B	0.46	1.00 (5)	0.72 (6)	0.81 (9)	0.42 (8)	0.40 (8)
Si	x	0.5000	0.5000	0.5000	0.5000	0.5000	0.5000
	y	0.0000	0.0000	0.0000	0.0000	0.0000	0.0000
	z	0.5000	0.5000	0.5000	0.5000	0.5000	0.5000
	B	0.25	0.66 (3)	0.37 (4)	0.51 (7)	0.31 (4)	0.40 (8)
O1	x	0.1028 (2)	0.1031 (12)	0.1007 (15)	0.1019 (24)	0.1021 (10)	0.0991 (16)
	y	0.4660 (2)	0.4654 (9)	0.4637 (11)	0.4627 (20)	0.4648 (13)	0.4640 (22)
	z	0.2500	0.2500	0.2500	0.2500	0.2500	0.2500
	B	0.32	0.67 (9)	0.77 (11)	0.87 (19)	0.25 (13)	0.23 (19)
O2	x	0.1961 (1)	0.1953 (7)	0.1979 (8)	0.1976 (14)	0.1954 (6)	0.1964 (10)
	y	0.2014 (2)	0.2010 (6)	0.2026 (7)	0.2014 (12)	0.2019 (8)	0.2012 (13)
	z	0.5531 (1)	0.5510 (4)	0.5524 (5)	0.5518 (7)	0.5547 (12)	0.5612 (19)
	B	0.34	0.66 (6)	0.44 (7)	0.41 (12)	0.41 (9)	0.08 (14)

[a] Horiuchi et al. (1987); [b] This study, in diamond anvil cell

approximately 23% less compressible than a or c which had very similar compressibilities (Fig. 1). The axial compressibilities calculated from unweighted, least-squares fit of the compression data yields axial compressibilities of $1.30(2)\times10^{-3}$ GPa^{-1}, $1.04(3)\times10^{-3}$ GPa^{-1} and $1.24(2)\times10^{-3}$ GPa^{-1} for a, b and c, respectively. The figures in the parentheses represent one estimated standard deviation of the least-squares fit. If errors of 0.1 GPa for pressure uncertainty are included, the axial compressibilities are: $1.30(5)\times10^{-3}$ GPa^{-1}, $1.04(4)\times10^{-3}$ GPa^{-1}, and $1.24(4)\times10^{-3}$ GPa^{-1}. Thus the compressibility of a and c are not significantly different.

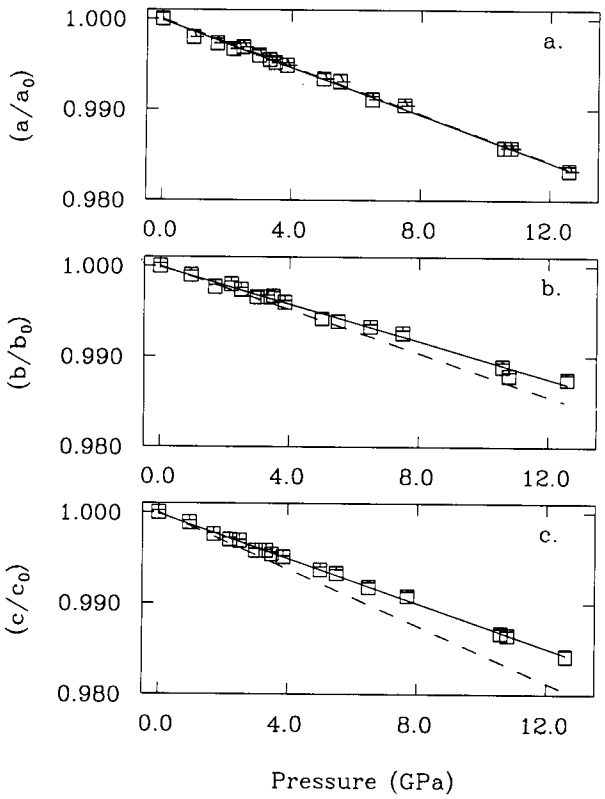

Fig. 1. The variation of (**a**) a/a_0, (**b**) b/b_0, and (**c**) c/c_0 with pressure. *Dashed lines* representing results from Brillouin spectroscopy are shown for comparison with axial compressibilities of this study (*symbols and solid lines*)

Results from other studies are presented for comparison in Table 4. The largest discrepancy is found between our study and the powder diffraction studies of Yagi et al. (1982) and Knittle and Jeanloz (1987). Pressure conditions in Yagi et al.'s (1982) study became nonhydrostatic between 7.5 and 9 GPa, thus only data below 7.5 GPa were used for compressibility calculations. The pressure conditions in the measurements of Knittle and Jeanloz (1987) were nonhydrostatic. Moreover, the relative compressibilities of the lattice parameters could not be accurately determined since there was inadequate resolution to separate the orthorhombic splitting of equivalent cubic diffraction peaks. Recently, Mao et al. (1989) used monochromatic synchrotron X-ray radiation to obtain high resolution powder diffraction data to measure the lattice parameters of $(Mg,Fe)SiO_3$ perovskite at high

Table 4. Comparison of experimental determinations of the zero-pressure bulk modulus, K_T, and linear compressibilities of $a(\beta_a)$, $b(\beta_b)$, and $c(\beta_c)$, for $MgSiO_3$ perovskite at 298 K

K_T (GPa)	K'_T	β_a (GPa^{-1})	β_b (GPa^{-1})	β_c (GPa^{-1})	Sample	Ref.
246	–	0.00131	0.00120	0.00156	single crystal	1
247	4	0.00141	0.00107	0.00157	single crystal	2
254	4	0.00130	0.00104	0.00124	single crystal	3
258	4	0.00158	0.00119	0.00110	powder	4
266	3.9	–	–	–	powder	5
272	4	0.00129	0.00105	0.00133	powder	6

References: 1. Yeganeh-Haeri et al. (1990); 2. Kudoh et al. (1987); 3. This study; 4. Yagi et al. (1982); 5. Knittle and Jeanloz (1987); 6. Mao et al. (1989)

pressures and temperatures. They were able to resolve the triplet consisting of the 020, 112, and 200 diffraction lines which are equivalent to the 110 diffraction peak of cubic perovskite. They found that b was approximately 25% less compressible than a or c which had similar compressibilities (Table 4). Results from the Mao et al.'s (1989) study show excellent agreement with our study. Kudoh et al. (1987) studied several single crystals at high pressure and found compressibilities of the cell parameters varied as follows: $c>a>b$ for crystal # 2, $a>c>b$ for crystal # 3, and $c>a\approx b$ for crystal # 4. This variation may reflect the fact that their room pressure values for a, b and c were determined from an average of three room-pressure unit-cells: from crystal # 4 in the diamond anvil cell, from crystal # 1 in air, and from Horiuchi et al.'s (1987) results. Results from this study, Mao et al.'s (1989) study and Kudoh et al.'s (1987) study, however, all agree that b is the least compressible axis. Consequently, the axial ratios, a/b and c/b, increase with pressure.

Single-crystal Brillouin spectroscopy by Yeganeh-Haeri et al. (1989) suggests the compressibility of c is greater than a which is slightly greater than b (Table 4). These data should, in principle, be more accurate than compression studies. They are, however, appropriate for very low pressures. It is interesting that at low pressures our data, within the experimental uncertainty of our data, show reasonable agreement with the Brillouin data (Fig. 1). At pressures above 4 GPa, however, the compressibility data, especially for b and c, deviate from the slopes of the compressibility curves calculated from the acoustic experiments. This finding is consistent with our observations of the structural response of $MgSiO_3$ perovskite to pressure discussed in detail below.

$MgSiO_3$ Perovskite Bulk Modulus

The variation of the molar volume of $MgSiO_3$ perovskite with pressure is shown in Fig. 2. The pressure-volume data from the three crystals were combined for a least-squares fit of a Birch-Murnaghan equation of state,

$$P=\tfrac{3}{2}K_T[(V_0/V)^{\frac{7}{3}}-(V_0/V)^{\frac{5}{3}}]\,[1-\tfrac{3}{4}(4-K_T')]\,[(V_0/V)^{\frac{2}{3}}-1] \quad (1)$$

where P, V_0, V, K_T and K' are the pressure, molar volume at room pressure, molar volume at pressure, bulk modulus, and pressure derivative of the bulk modulus, respectively. Since the total range of volume compression is less than 5%, the data were constrained by fixing K_T' equal to 4 and V/V_0 equal to 1.00 at room pressure. Using all of the data, a value of 254(13) GPa was obtained for K_T. Similar results were obtained by fitting a Murnaghan equation of state to the data.

The isothermal bulk modulus determined from this study is compared with those from other studies in Table 4. The various determinations of the bulk modulus from compressibility studies range from 247 GPa to 272 GPa. The total difference in uncertainty, however, is within the experimental uncertainties of each study. In fact, the difference is much smaller than those typically

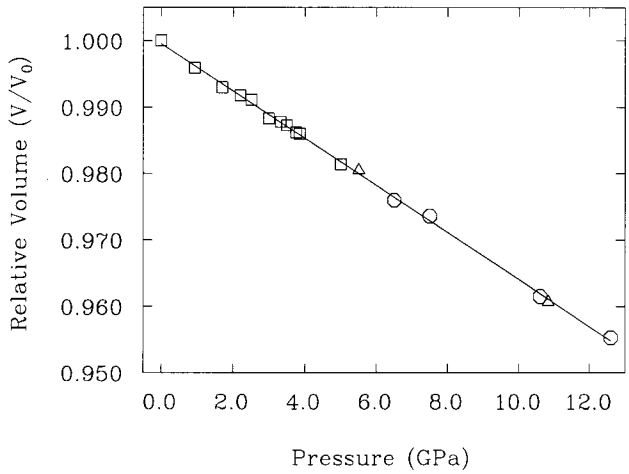

Fig. 2. Room-temperature compression of $MgSiO_3$ perovskite. *Squares* represent results from crystal # 1 (both mounts), *triangles* represent results from crystal # 2 and *circles* represent results from crystal # 3

observed in other materials when interlaboratory comparisons are made. Pressure-volume data do not provide very strong constraints on the bulk modulus since there are so many free variables in the Birch-Murnaghan equation of state (including K_T' and the zero-pressure volume) combined with the fact that the total compression being measured is small. In order to decrease the number of free variables, values of K_T' are assumed, as described above. Brillouin spectroscopy experiments should provide a much more reliable value for the bulk modulus since they measure the elastic moduli directly. Yeganeh-Haeri et al. (1987) obtained a value for the adiabatic bulk modulus, K_S, of 246(1) GPa from Brillouin spectroscopy. The isothermal bulk modulus, K_T, is related to the adiabatic bulk modulus, K_S, by

$$K_T=\frac{K_S}{1+\alpha\gamma T} \quad (2)$$

where α is the thermal expansion coefficient and γ is the Gruneisen parameter. Substitution of α at 300 K, $2.20\times10^{-5}\ K^{-1}$ (Ross and Hazen 1989), and γ, 1.9 (Hemley et al. 1989), into equation (2) yields a value of 243 GPa for K_T which is less than the lowest determination of K_T from compressibility measurements (Table 4).

$MgSiO_3$ Perovskite Crystal Structure at High Pressure

There has been considerable interest whether the degree of orthorhombic distortion in $MgSiO_3$ perovskite will increase or decrease at pressures characteristic of Earth's lower mantle. Yagi et al. (1978) suggested that $MgSiO_3$ perovskite should tend toward cubic symmetry with increasing pressure. They argued that the ratio of effective ionic radii, $R_A/(R_B+R_O)$, would increase under pressure because the oxygen anion is more compressible than the cations. Thus the cubic form would be favored at high pressure. O'Keeffe et al. (1979), on the other hand, argued that the perovskite structure would not favor the cubic

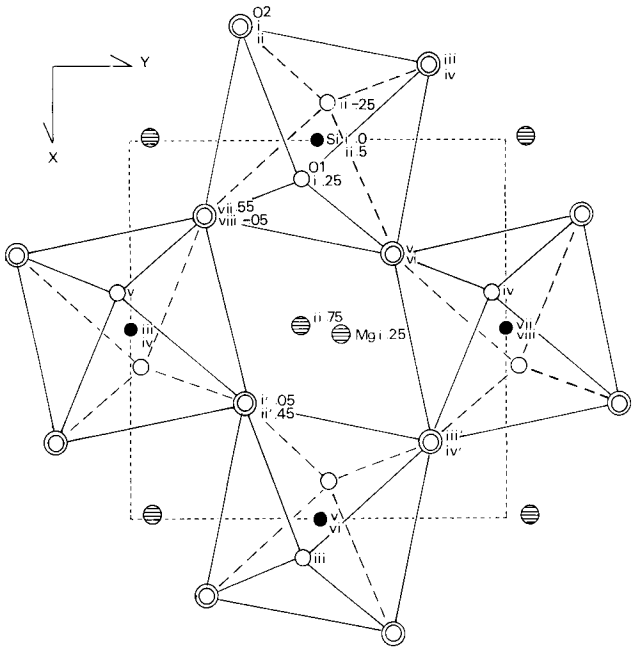

Fig. 3. Room-pressure, room-temperature structure of $MgSiO_3$ perovskite projected on (001); Mg sites are ruled, Si sites are solid, O(1) sites are open and O(2) sites are doubled. Each atom is numbered with lower-case Roman numerals

form at high pressure. They derived a relationship between the angle of rotation of the SiO_6 octahedron about its three-fold axis in terms of the relative compressibilities of the Mg–O and Si–O bonds. They argued that the ratio, $(R_A+R_O)/(R_B+R_O)$, would decrease with pressure and would thus give rise to larger tilting of SiO_6 octahedra and increased distortion with pressure. A recent theoretical study of the structure of $MgSiO_3$ perovskite at pressure (Hemley et al. 1987) supports O'Keeffe et al.'s (1979) analysis, predicting a general increase in the degree of distortion with compression. Kudoh et al. (1987) observed that pressure moves coordination of Mg towards 8-fold, rather than 12-fold coordination, consistent with the two latter studies.

A projection of the room temperature, room pressure structure of $MgSiO_3$ perovskite is shown in Fig. 3. Between 0 and 5 GPa, the primary response of the structure is through compression of the Si–O and Mg–O bonds (Tables 5 and 6) resulting in the decrease of the volumes of the Si octahedron and Mg dodecahedron (Fig. 4). Above 5 GPa, the bonds continue to shorten and the SiO_6 polyhedral bulk modulus calculated between 0 and 12.6 GPa is 333 GPa, similar to the value obtained for SiO_6 in stishovite (Ross et al. 1990). In addition to compression of the Si–O and Mg–O bonds above 5 GPa, the SiO_6 octahedra begin to tilt. Tilting in the $[ab]$ plane is reflected in the decrease of the $Si^{i}-O(2)^{viii}-Si^{iii}$ (Fig. 6) and $O(2)^{i}-O(2)^{viii}-O(2)^{i'}$ angles (Table 7). This is accompanied by a smaller degree of tilting in the $[bc]$ plane as indicated by the increase in $O(2)^{i'}-O(2)^{ii'}-O(2)^{vii}$ and $Si^{i}-O(1)^{i}-Si^{ii}$ angles (Table 7). This onset of tilting of the SiO_6 octahedra above 5 GPa coincides with the divergence of the axial compressibilities from the acoustic measurements (Fig. 1).

Sasaki et al. (1983) formulated a way to describe the tiltings and distortions in $GdFeO_3$-type perovskites such as $MgSiO_3$ perovskite in a systematic way. They defined the observed tolerance factor, t_{obs}, as follows:

$$t_{obs}=\frac{\langle A-O\rangle}{\sqrt{2}\langle B-O\rangle}, \tag{3}$$

where $\langle A-O\rangle$ and $\langle B-O\rangle$ are the mean interatomic distances with twelve and six coordination for A (e.g. Mg) and B (e.g. Si) sites, respectively. The t_{obs} values for $MgSiO_3$ perovskite calculated at different pressures are listed in Table 6. The observed tolerance factor shows no change between 0 and 5 GPa, but displays a small decrease above 5 GPa, signifying an increase in distortion ($t_{obs}=1.0$ for an ideal cubic perovskite). Thus the

Table 5. Interatomic distances (Å) and angles (°) in Si octahedra. Standard deviations are in parentheses

Pressure (GPa):		0.0	2.2	5.0	7.5	10.6
Si i–O(1) i	x2	1.801 (1)	1.794 (2)	1.790 (3)	1.784 (1)	1.773 (2)
Si i–O(2) v	x2	1.795 (4)	1.787 (4)	1.777 (6)	1.787 (4)	1.783 (6)
Si i–O(2) viii	x2	1.779 (3)	1.777 (4)	1.773 (6)	1.767 (4)	1.775 (7)
Mean ⟨Si–O⟩		1.792	1.786	1.780	1.779	1.777
Δ_B		0.027	0.015	0.017	0.025	0.006
O(1) i–O(2) v	x2	2.566 (4)	2.574 (5)	2.559 (8)	2.568 (8)	2.598 (13)
O(1) i–O(2) iv	x2	2.572 (5)	2.561 (7)	2.564 (11)	2.534 (7)	2.500 (11)
O(1) i–O(2) i'	x2	2.520 (6)	2.489 (7)	2.485 (11)	2.480 (8)	2.428 (12)
O(1) i–O(2) viii	x2	2.491 (3)	2.487 (4)	2.474 (6)	2.487 (7)	2.518 (12)
O(2) v–O(2) viii	x2	2.518 (1)	2.508 (2)	2.499 (3)	2.500 (1)	2.488 (2)
O(2) v–O(2) iv	x2	2.536 (2)	2.532 (2)	2.522 (4)	2.526 (5)	2.543 (9)
Mean ⟨O–O⟩		2.534	2.525	2.517	2.516	2.513
O(1) i–Si i–O(2) viii		88.2 (2)	88.3 (2)	88.0 (3)	88.9 (3)	90.3 (1)
O(1) i–Si i–O(2) v		91.0 (2)	91.9 (33)	91.7 (4)	92.0 (3)	93.7 (3)
O(2) v–Si i–O(2) viii		89.59 (5)	89.45 (6)	89.5 (1)	89.4 (1)	88.6 (2)
O(2) i–Si i–O(2) viii		90.41 (5)	90.55 (6)	90.5 (1)	90.6 (1)	91.4 (4)

Table 6. Interatomic distances (Å) for cuboctahedron. Standard deviations are in parentheses

Pressure (GPa):		0.0	2.2	5.0	7.5	10.6
Mg i–O(1) i	x1	2.009 (7)	2.029 (8)	2.013 (13)	1.999 (7)	1.994 (11)
Mg i–O(1) iv	x1	2.091 (5)	2.073 (6)	2.069 (11)	2.070 (7)	2.052 (11)
Mg i–O(1) iii	x1	2.853 (7)	2.825 (8)	2.822 (13)	2.820 (7)	2.804 (11)
Mg i–O(1) v	x1	2.963 (5)	2.970 (6)	2.958 (11)	2.947 (6)	2.934 (10)
Mg i–O(2) i′	x2	2.061 (4)	2.058 (4)	2.046 (7)	2.029 (6)	1.997 (10)
Mg i–O(2) iv′	x2	2.292 (4)	2.258 (5)	2.263 (8)	2.252 (6)	2.222 (9)
Mg i–O(2) v	x2	2.411 (3)	2.423 (4)	2.410 (6)	2.412 (8)	2.438 (12)
Mg i–O(2) viii	x2	3.111 (3)	3.107 (4)	3.092 (7)	3.101 (6)	3.113 (10)
Mean $\langle Mg-O\rangle^{VIII}$		2.204	2.198	2.190	2.182	2.170
Mean $\langle Mg-O\rangle^{XII}$		2.472	2.466	2.457	2.452	2.444
Δ_A		26.9	27.0	27.0	27.9	29.6
t_{obs}		0.976	0.976	0.976	0.974	0.972
O(1) i–O(1) v	x2	2.835 (6)	2.840 (7)	2.824 (11)	2.818 (5)	2.821 (8)
O(1) v–O(1) iii	x2	4.177 (9)	4.148 (11)	4.142 (18)	4.134 (8)	4.093 (12)
O(1) v–O(2) vii	x4	2.566 (4)	2.574 (5)	2.559 (8)	2.568 (8)	2.598 (13)
O(1) v–O(2) ii′	x4	2.572 (5)	2.561 (7)	2.564 (11)	2.534 (7)	2.500 (11)
O(1) iv–O(2) iii′	x4	2.520 (6)	2.489 (7)	2.485 (11)	2.480 (8)	2.428 (12)
O(1) iv–O(2) vi	x4	2.491 (3)	2.487 (4)	2.474 (6)	2.487 (7)	2.518 (12)
O(2) i′–O(2) ii′	x2	2.745 (6)	2.717 (6)	2.718 (10)	2.669 (16)	2.570 (3)
O(2) vii–O(2) viii	x2	4.153 (6)	4.160 (6)	4.137 (10)	4.164 (16)	4.237 (26)
O(2) i′–O(2) iv′	x4	2.518 (1)	2.508 (2)	2.499 (3)	2.500 (1)	2.488 (2)
O(2) iii′–O(2) vi	x4	2.536 (2)	2.532 (2)	2.522 (4)	2.526 (5)	2.543 (9)
O(2) i′–O(2) iii′	x4	3.725 (4)	3.697 (5)	3.692 (8)	3.657 (12)	3.577 (18)
O(2) i′–O(2) vii	x4	4.223 (7)	4.209 (8)	4.195 (1)	4.182 (1)	4.166 (1)
O(2) i′–O(2) v	x2	2.811 (6)	2.836 (7)	2.814 (12)	2.807 (8)	2.822 (13)
O(2) iv′–O(2) viii	x2	4.201 (6)	4.165 (7)	4.159 (12)	4.169 (7)	4.166 (12)

results from this study support Hemley et al.'s (1987) calculations and the crystal chemical arguments of O'Keeffe et al. (1979). The degree of distortion from ideal cubic symmetry in $MgSiO_3$ perovskite increases as a function of pressure.

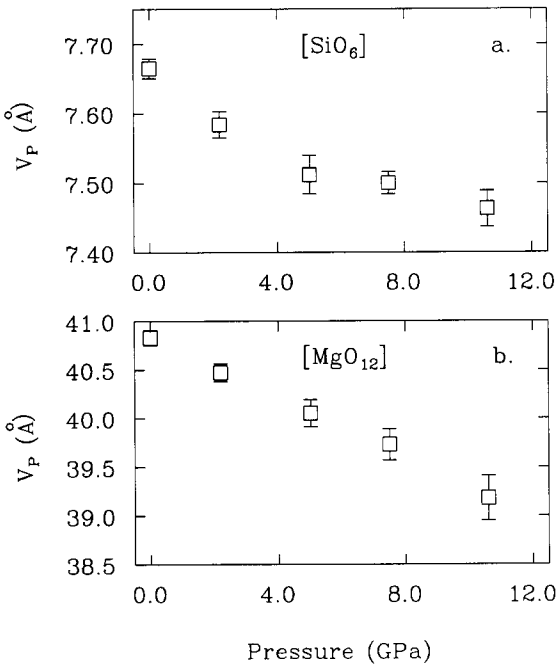

Fig. 4. Plot of the polyhedral volume of (**a**) the SiO_6 octahedron and (**b**) the MgO_{12} dodecahedron as a function of pressure

Although the most prominent distortion with pressures greater than 5 GPa is tilting of the polyhedra, the degree of distortion within the polyhedra also changes under compression. The bond length distortion factor (Sasaki et al. 1983),

$$\Delta = \frac{1}{n}\sum\left[\frac{(r_i - r)^2}{r}\cdot 10^3\right], \tag{4}$$

provides a measure of this distortion. The Mg cuboctahedron, which is very distorted at room temperature and pressure ($\Delta_A = 26.9$), shows an increase in distortion with pressure to 29.6 at 10.6 GPa (Table 6). The value of Δ_B

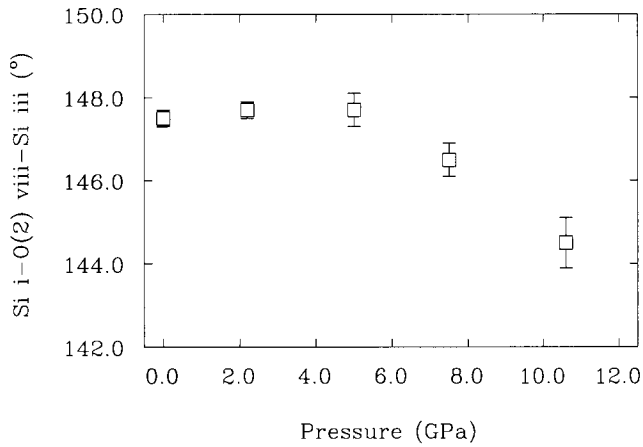

Fig. 5. Variation of the $Si^{i}-O(2)^{viii}-Si^{iii}$ with pressure, showing the increased tilting of SiO_6 octahedra in the *ab*-plane

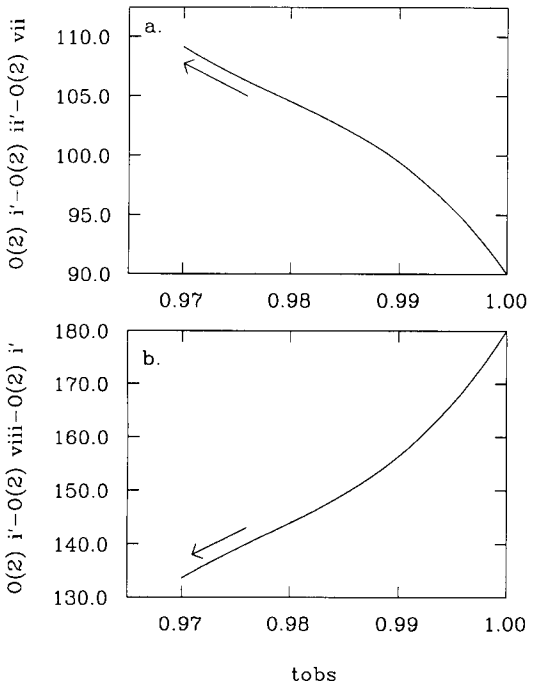

Fig. 6. The trends of (**a**) $O(2)^{i'}-O(2)^{ii'}-(O(2)^{vii}$ vs. t_{obs} and (**b**) $O(2)^{i}-O(2)^{viii}-O(2)^{i'}$ vs. t_{obs} for the $GdFeO_3$-type perovskites (see Sasaki et al. 1983). The ideal cubic perovskite structure has $t_{obs}=1.000$. The *arrows* show the changes observed in $MgSiO_3$ perovskite with increasing pressure and are in the direction of increasing distortion

for the Si octahedron, however, shows no systematic variation with pressure (Table 5).

Several trends between t_{obs} and the angles showing tilting of polyhedra and distortions of polyhedra are apparent in $MgSiO_3$ perovskite as a function of pressure. First, as pressure increases, t_{obs} decreases, concommittant with a decrease in $O(2)^{i}-O(2)^{viii}-O(2)^{i'}$ (tilting in *ab*-plane). Second, the $O(2)^{i'}-O(2)^{ii'}-O(2)^{vii}$ angle (tilting in *bc*-plane) decreases with decreasing t_{obs} (increasing pressure). Third, as t_{obs} decreases, the bondlength distortion for the *A*-site, Δ_A, increases. There is no systematic relationship between decreasing t_{obs} and the bond-length distortion of the *B*-site, Δ_B. These observations conform with observed systematic relationships in $GdFeO_3$-type perovskites noted by Sasaki et al. (1983). Figure 6 shows the variation of $O(2)^{i}-O(2)^{viii}-O(2)^{i'}$ and $O(2)^{i'}-O(2)^{ii'}-O(2)^{vii}$ with t_{obs} in $MgSiO_3$ perovskite with increasing pressure. The polynomial equations formulated by Sasaki et al. (1983) from a number of $GdFeO_3$-type perovskites are included in Fig. 6. With an increase of 10.6 GPa, $MgSiO_3$ perovskite has undergone a degree of distortion similar to that found in $YFeO_3$. Sasaki et al.'s (1983) trends may provide a method to predict structural distortions in $GdFeO_3$-type perovskites with pressure. By 30 GPa, for example, it is likely that $MgSiO_3$ perovskite is approaching a structure as distorted as $InCrO_3$ ($t_{obs}=0.964$).

Conclusions

The conclusions from this study can be summarized as follows:

1. The compression of $MgSiO_3$ perovskite is anisotropic. The *b*-axis is least compressible and the compressibility of *a* and *c* are similar and are approximately 23% more compressible than *b*.

2. The isothermal bulk modulus obtained from the 15 pressure-volume data in this study is 254 GPa if V_0 is fixed and K' is set to 4. This value is consistent with previous determinations of the isothermal bulk modulus.

3. Between 0 and 5 GPa, the primary response of the structure to pressure is compression of the Mg–O and Si–O bonds. Above 5 GPa, the SiO_6 octahedra begin to tilt.

4. The degree of distortion from the ideal cubic perovskite structure increases with pressures greater than 5 GPa. With increasing pressure, the observed tolerance factor decreases, the tilt in the [*ab*]-plane decreases, the tilt in the [*bc*]-plane increases, and the bond-length distortion of the MgO_{12} site increases, thus following the

Table 7. Metal-metal distances (Å) and Si–O–Si, and O(2)–O(2)–O(2) angles (°) with standard deviations in parentheses

Pressure (GPa):	0.0	2.2	5.0	7.5	10.6
Si i–Si iii	3.4313 (2)	3.4225 (2)	3.4101 (3)	3.4028 (3)	3.4035 (3)
Si i–Si ii	3.4485 (2)	3.4385 (2)	3.4270 (3)	3.4165 (3)	3.3886 (3)
Mg i–Mg iii	3.520 (5)	3.527 (6)	3.511 (9)	3.495 (6)	3.464 (10)
Mg i–Mg v	3.345 (5)	3.321 (5)	3.312 (9)	3.313 (6)	3.315 (10)
Mg i–Mg ii	3.4950 (7)	3.4875 (8)	3.473 (1)	3.4637 (9)	3.450 (1)
Mg i–Si i	3.010 (3)	3.011 (3)	2.998 (5)	2.984 (4)	2.962 (6)
Mg i–Si iii	3.239 (2)	3.235 (2)	3.217 (3)	3.215 (2)	3.203 (4)
Mg i–Si v	2.908 (3)	2.891 (3)	2.882 (5)	2.879 (4)	2.875 (6)
Mg i–Si vii	2.785 (2)	2.774 (2)	2.770 (3)	2.761 (2)	2.751 (3)
Si i–O(1) i–Si ii	146.4 (3)	146.8 (4)	146.4 (7)	146.6 (3)	147.3 (5)
Si i–O(2) viii–Si iii	147.5 (2)	147.7 (4)	147.7 (4)	146.5 (4)	144.5 (6)
O(2) i–O(2) viii–O(2) i'	140.7 (2)	140.3 (3)	140.4 (5)	139.1 (6)	135.7 (1.0)
O(2) viii–O(2) i'–O(2) iv'	112.4 (2)	111.5 (1)	111.8 (4)	112.1 (2)	111.8 (3)
O(2) i'–O(2) ii'–O(2) vii	106.1 (1)	106.5 (1)	106.3 (2)	107.2 (4)	109.1 (6)

systematic relationships amoung $GdFeO_3$-type perovskites.

Acknowledgments. We thank Drs. E. Ito (Okayama University) and D.J. Weidner (SUNY at Stony Brook) for synthesizing and supplying the single crystals that made this study possible. This paper has benefitted from critical reviews of Dr. Y. Kudoh, Dr. D. Weidner and an anonymous reviewer, as well as suggestions by Drs. C.T. Prewitt and R.J. Hemley. Support for this work came from NSF grants EAR-8419982 and EAR-8608946 (RMH). NLR gratefully acknowledges support from NSF grant EAR-8618602 awarded to Dr. C.T. Prewitt.

References

Anderson OL (1976) The 650 km mantle discontinuity. Geophys Res Lett 3:347–349

Choudhury N, Chaplot SL, Rao KR, Ghose S (1988) Lattice dynamics of $MgSiO_3$ perovskite. Pramana – J Phys 30:423–428

Cohen RE (1987) Elasticity and equation of state of $MgSiO_3$ perovskite. Geophys Res Lett 14:1053–1056

Finger LW, Prince E (1975) A system of Fortran IV computer programs for crystal structure computations. US Natl Bur Stand Tech Note 854, Washington DC, 129 p.

Hazen RM, Finger LW (1978) Crystal structures and compressibilities of pyrope and grossular to 60 kbar. Am Mineral 63:297–303

Hazen RM, Finger LW (1981) Calcium fluoride as an internal pressure standard in high-pressure/high-temperature crystallography. J Appl Crystallogr 14:234–236

Hazen RM, Finger LW (1982) Comparative Crystal Chemistry. Wiley, New York, pp 5–16

Heinz DL, Jeanloz R (1987) Measurement of melting curve of $Mg_{0.9}Fe_{0.1}SiO_3$ at lower mantle conditions and its geophysical implications. J Geophys Res 92:11437–11444

Hemley RJ, Jackson MD, Gordon RG (1987) Theoretical study of the structure, lattice dynamics, and equations of state of perovskite-type $MgSiO_3$ and $CaSiO_3$. Phys Chem Minerals 14:2–12

Hemley RJ, Cohen RE, Yeganeh-Haeri A, Mao HK, Weidner DJ, Ito E (1989) Raman spectroscopy and lattice dynamics of $MgSiO_3$-perovskite at high pressure. Proc Chapman Conf on Perovskites, Am Geophys Union, Washington, DC

Hofmeister AM, Williams Q, Jeanloz R (1987) Thermodynamic and elastic properties of $MgSiO_3$ perovskite from far-IR spectra at pressure. EOS Trans Am Geophys Union 68:1469

Horiuchi H, Ito E, Weidner DJ (1987) Perovskite-type $MgSiO_3$: single-crystal x-ray diffraction study. Am Mineral 72:357–360

International Tables for X-ray Crystallography (1974) Kynoch Press, Birmingham

Ito E (1977) The absence of oxide mixture in high-pressure phases of Mg-silicate. Geophys Res Lett 4:72–74

Ito E (1982) Ultra-high pressure phase relations of the system $MgO-FeO-SiO_2$ and their geophysical implications. In: Sunagawa I (ed) Materials Science of the Earth's Interior, Terra Tokyo, pp 389–396

Ito E, Matsui Y (1977) Silicate ilmenites and the post-spinel transformation. In: Manghnani M, Akimoto S (eds) High-Pressure Research Applications in Geophysics. Academic New York, pp 93–208

Ito E, Matsui Y (1978) Synthesis and crystal-chemical characterization of $MgSiO_3$ perovskite. Earth Planet Sci Let 38:443–450

Ito E, Matsui Y (1979) High-pressure transformation in silicates, germanates and titanates with ABO_3 stoichiometry. Phys Chem Mineral 4:265–273

Ito E, Weidner DJ (1986) Crystal growth of $MgSiO_3$ perovskite. Geophys Res Lett 13:464–466

Ito E, Takahashi E, Matsui Y (1984) The mineralogy and chemistry of the lower mantle: an implication of the ultrahigh-pressure phase relations in the system $MgO-FeO-SiO_2$. Earth Planet Sci Lett 67:238–248

Jackson WE, Knittle E, Brown GE Jr, Jeanloz R (1987) Partitioning of Fe within high-pressure silicate perovskite: evidence for unusual geochemistry in the lower mantle. Geophys Res Lett 14:224–226

Jephcoat AP, Mao HK, Bell PM (1987) Operation of the megabar diamond-anvil cell. In: Ulmer GC, Barnes HL (eds) Hydrothermal Experimental Techniques. Wiley New York, pp 469–506

King HE, Finger LW (1979) Diffracted beam crystal centering and its application to high-pressure crystallography. J Appl Cryst 12:374–378

Knittle E, Jeanloz R (1987) Synthesis and equation of state of $(Mg,Fe)SiO_3$ perovskite to over 100 Gigapascals. Science 235:668–670

Knittle E, Jeanloz R, Smith GL (1986) Thermal expansion of silicate perovskite and stratification of the Earth's mantle. Nature 319:214–216

Kudoh Y, Ito E, Takeda H (1987) Effect of pressure on the crystal structure of perovskite-type $MgSiO_3$. Phys Chem Minerals 14:350–354

Levien L, Prewitt CT, Weidner DJ (1979) Compression of pyrope. Am Mineral 64:805–808

Li X, Jeanloz R (1987) Electrical conductivity of $(Mg,Fe)SiO_3$ perovskite and a perovskite dominated assemblage at lower mantle conditions. Geophys Res Lett 14:1075–1078

Liu LG (1974) Silicate perovskite from phase transformations of pyrope-garnet at high pressure and temperature. Geophys Res Lett 1:277–280

Liu LG (1975a) Post-oxide phases of forsterite and enstatite. Geophys Res Lett 2:417–419

Liu LG (1975b) Post-oxide phases of olivine and pyroxene and mineralogy of the mantle. Nature 258, 510–512

Liu LG (1976a) The post-spinel phase of forsterite. Nature 262:770–772

Liu LG (1976b) The high-pressure phases of $MgSiO_3$. Earth Planet Sci Lett 31:200–208

Liu LG (1976c) Orthorhombic perovskite phases observed in olivine, pyroxene and garnet at high pressures and temperatures. Phys Earth Planet Int 11:289–298

Liu LG (1977) Mineralogy and chemistry of the earth's mantle above 1000 km. Geophys J Roy Astr Soc 48:53–62

Liu LG (1979) On the 650-km seismic discontinuity. Earth Planet Sci Lett 42:202–208

Liu LG, Ringwood AE (1975) Synthesis of a perovskite-type polymorph of $CaSiO_3$. Earth Planet Sci Lett 28:209–211

Mao HK, Yagi T, Bell PM (1977) Mineralogy of the earth's deep mantle: quenching experiments of mineral compositions at high pressure and temperature. Carnegie Inst Wash Year Book 76:502–504

Mao HK, Hemley RJ, Shu J, Chen L, Jephcoat AP, Bassett WA (1989) The effect of pressure, temperature, and composition on lattice parameters and density of $(Fe,Mg)SiO_3$-perovskite to 30 GPa. Carnegie Inst Wash Year Book, 1988–1989:82–89

Marezio M, Remeika JP, Jayaraman A (1966) High-pressure decomposition of synthetic garnets. J Chem Phys. 45:1821–1824

Matsui M, Akaogi M, Matsumoto T (1987) Computational model of the structural and elastic properties of the ilmenite and perovskite phases of $MgSiO_3$. Phys Chem Minerals 14:101–106

Mills RL, Liebenberg DH, Bronson JC, Schmidt LC (1980) Procedure for loading diamond cells with high-pressure gas. Rev Scien Instrum 51:891–895

Miyamoto M (1988) Ion migration in $MgSiO_3$-perovskite and olivine by molecular dynamics calculations. Phys Chem Minerals 15:601–604

Miyamoto M, Takeda H (1984) An attempt to simulate high pressure structures of Mg-silicates by an energy minimization method. Am Mineral 69:711–718

O'Keeffe M, Hyde BG, Bovin J-O (1979) Contribution to the crystal

chemistry of orthorhombic perovskites: $MgSiO_3$ and $NaMgF_3$. Phys Chem Minerals 4:299–305

Ralph RL, Finger LW (1982) A computer program for refinement of crystal orientation matrix and lattice constants from diffractometer data with lattice symmetry constraints. J Appl Crystallogr 15:537–539

Reid AF, Ringwood AE (1975) High-pressure modification of $ScAlO_3$ and some geophysical implications. J Geophys Res 80:3363–3369

Ringwood AE (1962) Mineralogical constitution of the deep mantle. J Geophys Res 67:4005–4010

Ringwood AE (1966) Mineralogy of the mantle. In: Hurley PM (ed) Advances in the Earth Sciences. MIT Press Cambridge, pp 357–398

Ringwood AE, Major A (1967) Some high-pressure transformations of geophysical significance. Earth Planet Sci Lett 2:106–110

Ringwood AE, Major A (1971) Synthesis of majorite and other high pressure garnets and perovskites. Earth Planet Sci Lett 12:411–418

Ross NL, Hazen RM (1989) Single crystal X-ray diffraction study of $MgSiO_3$ perovskite from 77 to 400 K. Phys Chem Minerals 16:415–420

Ross NL, Shu J, Hazen RM (1990) High-pressure crystal chemistry of stishovite (in press)

Sasaki S, Prewitt CT, Liebermann RC (1983) The crystal chemistry of $CaGeO_3$ perovskite and the crystal chemistry of $GdFeO_3$-type perovskites. Am Mineral 68:1189–1198

Sawamoto H (1977) Orthorhombic pervoskite $(Mg,Fe)SiO_3$ and constitution of the lower mantle. In: Manghnani MH, Akimoto S (eds) High-pressure research Applications in Geophysics. Academic NY, pp 219–244

Swanson DK, Weidner DJ, Prewitt CT, Kandelin JJ (1985) Single crystal compression of $\gamma-Mg_2SiO_4$ (abstract). EOS Trans Am Geophys Union 66:370

Wall A, Price GD, Parker SC (1986) A computer simulation of the structure and elastic properties of $MgSiO_3$ perovskite. Mineral Mag 50:693–707

Weng K, Xu J, Mao HK, Bell PM (1983) Preliminary fourier-transform infrared spectral data on the SiO_6^{8-} octahedral group in silicate perovskite. Carnegie Inst Wash Year Book 82:355–356

Williams Q, Jeanloz R, McMillan P (1987) Vibrational spectrum of $MgSiO_3$ perovskite: zero-pressure Raman and mid-infrared spectra to 27 GPa. J Geophys Res 92:8116–8128, 11670

Wolf GH, Bukowinski MST (1985) Ab initio structural and thermoelastic properties of orthorhombic $MgSiO_3$ perovskite. Geophys Res Lett 12:809–812

Wolf GH, Bukowinski MST (1987) Theoretical study of the structural properties and equations of state of $MgSiO_3$ and $CaSiO_3$ perovskites: Implications for lower mantle composition. In: Manghnani M, Syono Y (eds) High-Pressure Research in Geophysics, Am Geophys Union, Washington, DC, pp 313–331

Yagi T, Mao HK, Bell PM (1978) Structure and crystal chemistry of perovskite-type $MgSiO_3$. Phys Chem Minerals 3:97–110

Yagi T, Bell PM, Mao HK (1979) Phase-relations in the system $MgO-FeO-SiO_2$ between 150 and 700 kbar at 1000°. Carnegie Inst Wash Year Book 78:614–618

Yagi T, Mao HK, Bell PM (1982) Hydrostatic compression of perovskite-type $MgSiO_3$. In: Saxena SK (ed) Advances in Physical Geochemistry. Springer Berlin Heidelberg New York, pp 317–325

Yeganeh-Haeri A, Weidner DJ, Ito E (1990) Single-crystal elastic moduli of magnesium metasilicate perovskite. In: Navrotsky A, Weidner DJ (eds) Perovskite: A Structure of Great Interest to Geophysics and Materials Science. Washington: Am Geophys Union (in press)